Diabatic Heating Model of the Indian Monsoon

G. C. ASNANI AND S. K. MISHRA

Indian Institute of Tropical Meteorology, Poona-5, India

(Manuscript received 25 April 1974; in revised form 23 September 1974)

ABSTRACT

In Part I of this paper, influence functions are derived for the response of a quasi-geostrophic atmosphere to transient heat sources and sinks, assuming that the effects of horizontal advection can be neglected and assuming a fairly reasonable vertical distribution of static stability. The influence is studied for diabatic heating of different horizontal wavelengths and for two different types of the vertical distribution. In Type I, heating is largest at the ground, decreasing to zero at $p=0$. In Type II, heating is maximum in the middle atmosphere and decreases parabolically to zero at $p=0$ and at the ground. It is shown that, in both types, the horizontal wavelength L of the heating function is very important in determining not only the intensity of pressure fall in the lower levels and of pressure rise aloft in the region of heating, but also the level of maximum pressure effect. It is seen that wavelengths of the order of 15,000 km produce maximum geopotential variations around the 150-mb level.

Introduction of Ekman layer friction decreases the intensity of pressure fall in the lower layers, increases the intensity of pressure rise aloft, lowers the level of phase reversal, and introduces a phase lag between the high pressure wave aloft and the low pressure wave below.

Part II deals with the application of theoretical results obtained in Part I to the problem of the Indian monsoon. It is visualized that the 12-monthly monsoon oscillation in southeast Asia is a linear perturbation on the annual mean flow pattern, the perturbation being essentially forced by differential diabatic heating in the horizontal plane; the perturbation is materially affected by low-level friction, while advection is assumed to be only of secondary importance.

In the first instance a 2-dimensional model of the monsoon in the y, p plane is constructed along the meridian 77.5°E, where observed annual mean conditions are taken as a basic state. On this is superimposed a linear perturbation forced by diabatic heating, sinusoidal in y and t and incorporating a combination of heating of Types I and II. The resulting total patterns of zonal wind in different months are presented. It is very encouraging to find that such a simple model, with only one wavelength in the y direction, is able to reproduce quite a few observed features of the zonal wind pattern in all months, including the westerly jet stream in winter and the easterly jet stream in summer.

1. Introduction

The monsoon of southeast Asia has been the subject of numerous studies. For a bibliography, one may consult Ramage (1971), who has listed over 400 references; others could be cited.

It appears that Jeffreys (1926) was the first to attack the problem of the monsoon in a quantitative manner. He considered a circular land area surrounded by an infinite ocean, the air over land being subjected to an annual cycle of diabatic heating and cooling. He incorporated the Coriolis parameter and neglected its variation with latitude. He also neglected friction. He was the first to point out, on the basis of his theory, that the amplitude of pressure oscillation depends on the horizontal dimensions of the land mass. His computed pressure amplitudes partly agreed with the observations (Coulson, 1931; Pisharoty and Asnani, 1958).

Böhme (1954a, 1954b, 1955) introduced turbulent transfer of heat from below and sinusoidal variation of the perturbation in the horizontal. His results were in good agreement with observations of annual pressure oscillation at the ground but widely differed with observations aloft (Pisharoty and Asnani, 1958). Later, numerical models of the general circulation (Phillips, 1956; Smagorinsky, 1963; Mintz and Arakawa, 1965; Manabe and Smagorinsky, 1967; Manabe *et al.*, 1970) were developed that simulated some observed features of the southeast Asian monsoon.

The present study does not intend to compete with such simulations. We have a very modest purpose. This is to isolate the influence of various forcings and to study the influence of diabatic heating and low-level friction separately when these are assumed to have simple idealized distributions in space and time, and to see the extent to which such simple patterns can explain the observed features of the Indian monsoon oscillation.

Heating is assumed to have sinusoidal variations in the horizontal and also in time. For the vertical distribution, two types of heating function are considered,

$$\left.\begin{aligned}\text{Type I: } Q_1 &= Q_G(p/p_0)^r e^{i(mx+ly)} \\ &\quad \times \sin\left(\frac{2\pi t}{\Gamma} - \frac{\alpha\pi}{180}\right) \\ \text{Type II: } Q_2 &= Q_H\{4p/p_0 - 4(p/p_0)^2\} e^{i(mx+ly)} \\ &\quad \times \sin 2\pi t/\Gamma\end{aligned}\right\}. \quad (1)$$

In (1), α is the phase difference in heating of Types I and II. The more common symbols have their usual meaning; others used in this article are listed below:

List of Symbols

A, A'	amplitude of constant-pressure geopotential wave in Eqs. (42, 43).
C	ps
c_p	specific heat of air at constant pressure
E	defined in Eq. (35a)
E_1	defined in Eq. (28)
E'	defined in Eq. (29)
F_{11}	defined in Eq. (31)
F_{12}	defined in Eq. (32)
F_2	defined in Eq. (33)
f_0	Coriolis parameter at 20° N
k	$f_0/2\sqrt{RC}$
K	eddy diffusivity
l, m	wavenumbers along x (eastward) and y axes
L	$2\pi(m^2+l^2)^{-\frac{1}{2}}$, effective wavelength in horizontal
p_0, p_f, p_r	pressures at 1000-mb level, at top of frictional (Ekman) layer, and at level of phase reversal
$Q_{\rm I}$, $Q_{\rm II}$	diabatic heating rates Q (per unit mass and time) defined in Eq. (1)
Q_G, Q_H	amplitudes of heating in Types I and II respectively
r	degree of polynomial in p/p_0 in heating of Type I, Eq. (1)
s	$(T/\theta)(\partial\theta/\partial p)$, static stability parameter
w_f	vertical velocity dz/dt at top of frictional (Ekman) layer
z	height of isobaric surface
α	phase difference in heating, expressed in degrees, Eq. (1)
α_0	angle of inflow at bottom of Ekman layer
ϵ, ϵ'	phase difference in isobaric geopotential, in radians, Eqs. (42, 43)
β	$\partial f/\partial y$ at 20°N
Γ	time period of oscillation
σ	angular frequency
λ	defined in Eq. (30)
μ	$(K/2)^{\frac{1}{2}} f_0^{-\frac{3}{2}} \sin 2\alpha_0$, frictional coefficient in Ekman layer
ν_1, ν_2	roots of $\nu^2+\nu-\pi^2/k^2L^2=0$, Eq. (26)
Φ	geopotential
ω	vertical velocity dp/dt in p-coordinate system, and its value at p_0
Ω	ω/p

It is generally accepted that there are essentially two types of vertical distribution of diabatic heating in the atmosphere. The first is through sensible heat exchange, which is largest at the earth-air interface. The heat gained by the atmosphere by this process decreases in the vertical. The other is generally believed to be through the latent heat released during condensation and this has a maximum in the middle atmosphere. Due to complexity of the physical processes involved in these diabatic heating processes, and to practical difficulties in the measurement and calculation of diabatic heat exchanges, there is at present no universally accepted profile of vertical distribution of diabatic heating. To simulate steady-state patterns through a quasi-geostrophic model on a spherical earth-surface, Sankar Rao and Saltzman (1969) assumed that the vertical profile of diabatic heating was essentially of Type I and also concluded that the most suitable value of r in $(p/p_0)^r$ appeared to be near 0.75. Several authors (Smagorinsky, 1953; Asakura and Katayama, 1964; Reed and Recker, 1971; Webster, 1972; Murakami, 1972; etc.) indicate a diabatic heating maximum in the middle and even the upper troposphere generally supporting heating of Type II. In the light of this experience of various workers, it is reasonable to assume both types of heating to be present. The vertical variation of $(p/p_0)^r$ for different values of r is shown in Fig. 1 (cf. Sankar Rao and Saltzman, 1969, Fig. 10).

Response of the atmosphere to variations of effective horizontal wavelength $L[=2\pi/(l^2+m^2)^{\frac{1}{2}}]$ for both types of heating and further, the response to the variations of r in heating of Type I, are studied systematically in some detail assuming that there is no horizontal advection. It is known that horizontal dimensions of the heating function play a part in the final influence

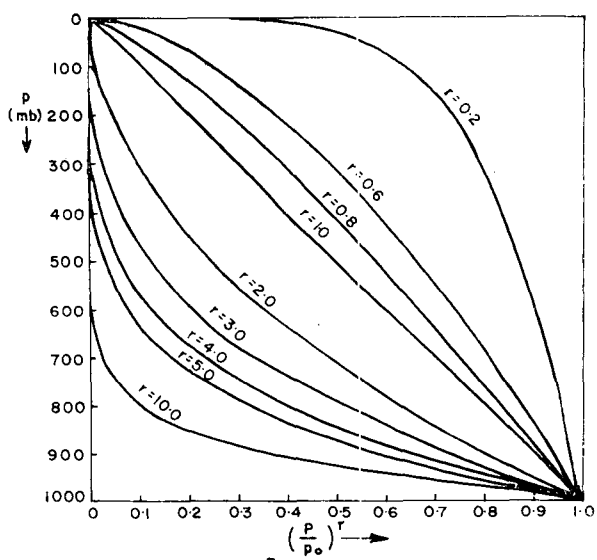

FIG. 1. Variation of $(p/p_0)^r$ with respect to p for different values of r.

on the atmosphere (Jeffreys, 1926; Döös, 1961; Sankar Rao and Saltzman, 1969; Derome and Wiin-Nielsen, 1971). The present work presents a more detailed and systematic analysis of the influence of L and r in the atmosphere but with the restriction that advective effects are neglected.

In general, heating produces low pressure in the lower levels and high pressure aloft with a level of phase reversal in the lower or middle troposphere. Analysis shows that without friction, the intensity of low pressure in the lower levels and of high pressure aloft was nearly the same whether the heating was of Type I or of Type II. Observational study of the annual monsoonal oscillation showed that, in the actual atmosphere, the intensity of high pressure aloft considerably exceeds that of low pressure at low levels during summer, the reverse occurring in winter. Also, observations showed a phase lag between the high pressure aloft and the low pressure below. A preliminary analysis showed that introduction of low-level friction in the model would reduce the intensity of the low-level system in relation to the high-level system and further produce a time lag between the two in the right direction, so that the model comes closer to the real atmosphere. We introduced low-level friction into the quasi-geostrophic model through frictionally-induced vertical motion in the Ekman boundary layer. For this, we adopted the simple model of Brunt (1941) presented in an elegant form by Charney and Eliassen (1949). We are aware of the objections that arise in respect to wholesale adoption of the Charney-Eliassen formulation for our model, which does not strictly satisfy the conditions stipulated for that formulation, namely barotropy and steady-state conditions in the Ekman layer. Time-dependency in Ekman layer theory has recently been introduced by Everson and Davies (1972), who suggest, among other minor variations, that in place of the Coriolis parameter f, we should use $(\sigma+f)$, where σ is the angular frequency and hence $2\pi/\sigma$ is the period of the phenomenon. Since our aim is to analyze periods that are very large compared to the inertial period, this sophistication is immaterial. In any case, the objection of adopting a steady-state formulation for time-dependent phenomena does not become serious in our case. Objection of barotropy, however, does persist. But in spite of this, the Charney-Eliassen formulation has been so widely used in meteorology with good success that our adopting the same does not appear to be highly objectionable. It has the advantage of amenability to easy adoption for analytical modeling.

In Part I, we have varied the frictional coefficient through a wide range of plausible values to study the differences in response of the atmosphere to varying degrees of friction at its bottom.

In Part II, we examine the degree to which the Indian monsoon can be explained as the direct result of seasonal heating variation in the absence of advective effects. The observed annual mean pattern along longitude 77.5°E is taken as a basic state for which explanation is not offered here. On this basic pattern, a linear perturbation, sinusoidal in y and t, is superimposed. The perturbation is imagined to be quasigeostrophic, entirely caused by diabatic heating with only one wavelength of 20,000 km in the y-direction from pole to pole, having no variation in the x-direction. Diabatic heating is assumed to be a mixture of Types I and II in suitable proportions. Ekman-layer friction is considered to be operative.

The resulting total pattern of zonal wind will be presented at 3-monthly intervals, for the region from 5°N to 35°N along 77.5°E. A number of features observed in the actual atmosphere in various months can then be easily recognized in these computed patterns. In particular, one finds the development of westerlies in the lower troposphere and of the easterly jet stream in the upper troposphere over south India with a proper slope during the summer season. The development of a westerly jet stream over north India during winter is also correctly reproduced. The phase differences between the low pressure at lower levels and the high pressure aloft during the summer season are predicted in the right sense. On the whole, it is very encouraging to find that such a simple and crude model as this should be able to reproduce faithfully a number of observed features of the annual oscillation. In the final result, our work has some similarity with that of Godbole (1973), who also simulated the July monsoon conditions in the y-p plane along approximately the central meridian of India; however, his method of simulation was quite different from ours.

Part I. Influence of diabatic heating

2. The model

a. *Tendency equation and ω-equation*

The vorticity and the thermodynamic equations of the quasi-geostrophic model with the β-plane approximation are well-known. These are:

$$\frac{\partial}{\partial t}\nabla^2\Phi+\frac{1}{f_0}J(\Phi,\nabla^2\Phi)+\beta\frac{\partial\Phi}{\partial x}-f_0^2\frac{\partial\omega}{\partial p}=0, \tag{2}$$

$$\frac{\partial}{\partial t}\frac{\partial\Phi}{\partial p}+\frac{1}{f_0}J\left(\Phi,\frac{\partial\Phi}{\partial p}\right)-\frac{Rs}{p}\omega+\frac{R}{pc_p}=0. \tag{3}$$

Notation is conventional; Q is the time rate of diabatic heat supplied to unit mass of air; $s\equiv(T/\theta)(\partial\theta/\partial p)$. Elimination of ω between (2) and (3) gives the geopotential tendency equation (4); elimination of $\partial\Phi/\partial t$ between these two equations gives the ω-equation (5):

$$\left[\nabla^2-\frac{f_0^2}{Rs}\left\{p\frac{\partial^2}{\partial p^2}+\left(1-\frac{p}{s}\frac{\partial s}{\partial p}\right)\frac{\partial}{\partial p}\right\}\right]\frac{\partial\Phi}{\partial t}$$
$$=J\left(\frac{1}{f_0}\nabla^2\Phi+f,\Phi\right)+\frac{f_0}{Rs}\left(1-\frac{p}{s}\frac{\partial s}{\partial p}\right)J\left(\Phi,\frac{\partial\Phi}{\partial p}\right)$$
$$+\frac{pf_0}{Rs}J\left(\Phi,\frac{\partial^2\Phi}{\partial p^2}\right)+\frac{f_0^2}{sc_p}\left(\frac{\partial Q}{\partial p}-\frac{1}{s}\frac{\partial s}{\partial p}Q\right), \quad (4)$$

$$\left(\nabla^2-\frac{pf_0^2}{Rs}\frac{\partial^2}{\partial p^2}\right)\omega=\frac{p}{f_0Rs}\left\{\nabla^2J\left(\Phi,\frac{\partial\Phi}{\partial p}\right)\right.$$
$$\left.-\frac{\partial}{\partial f}J(\Phi,\nabla^2\Phi)\right\}-\frac{\beta p}{f_0Rs}\frac{\partial}{\partial x}\frac{\partial\Phi}{\partial p}+\frac{1}{sc_p}\nabla^2Q=0. \quad (5)$$

b. Static stability assumptions

Energetic consistency of the quasi-geostrophic model (Lorenz, 1960) demands constancy of static stability along an isobaric surface. Examination of various static stability parameters in the troposphere over India (Asnani and Rao, 1963) shows that ps is nearly a constant. It is easy to appreciate this since

$$-ps=\frac{RT}{g}\left(\frac{g}{c_p}+\frac{\partial T}{\partial z}\right). \quad (6)$$

If the temperature lapse rate is constant, we shall have ps/T constant. Throughout the troposphere, T is of the same order of magnitude; hence ps will be nearly constant.

On similar considerations, ps will have another approximately constant value in each layer of the atmosphere having approximately constant lapse rate and not too large a variation in the value of T. Since the tropical troposphere contains nearly 90% of the total mass in a vertical column, we adopted a constant value of the static stability parameter,

$$-ps\equiv C=30\text{ K}, \quad (7a)$$

for the entire vertical column. It is hoped that different and more realistic values of C above the 100-mb level will not materially alter our conclusions. Further, in this notation,

$$-\frac{1}{\rho\theta}\frac{\partial\theta}{\partial p}=\frac{RC}{p^2}. \quad (7b)$$

With this assumption about the vertical variation of static stability, the term $-(p/s)\partial s/\partial p$ occurring in the tendency equation (4) becomes identically equal to unity, so that $1-(p/s)\partial s/\partial p=2$. Had we neglected vertical variation of s as has been done by some authors (Saltzman, 1965; Fisher and Wiin-Nielsen, 1971), this term would have taken half of this value. This particular representation of the static stability parameter in quasi-geostrophic models, first suggested by Kuo (1956), is not only quantitatively reasonable but also elegant for handling in analytical work. We further introduce the notation

$$k\equiv f_0/2(RC)^{\frac{1}{2}}, \quad (8)$$

$$\Omega\equiv\omega/p=\frac{d}{dt}\ln p. \quad (9)$$

Eqs. (4) and (5) then become

$$\left(p^2\frac{\partial^2}{\partial p^2}+2p\frac{\partial}{\partial p}+\frac{\nabla^2}{4k^2}\right)\frac{\partial\Phi}{\partial t}$$
$$=\frac{1}{4k^2}J\left(\frac{1}{f_0}\nabla^2\Phi+f,\Phi\right)-\frac{2p}{f_0}J\left(\Phi,\frac{\partial\Phi}{\partial p}\right)$$
$$-\frac{p^2}{f_0}J\left(\Phi,\frac{\partial^2\Phi}{\partial p^2}\right)-\frac{Rp}{c_p}\left(\frac{\partial Q}{\partial p}+\frac{Q}{p}\right), \quad (10)$$

$$\left(p^2\frac{\partial^2}{\partial p^2}+2p\frac{\partial}{\partial p}+\frac{\nabla^2}{4k^2}\right)\Omega$$
$$=-\frac{p}{f_0^3}\left\{\nabla^2J\left(\Phi,\frac{\partial\Phi}{\partial p}\right)-\frac{\partial}{\partial p}J(\Phi,\nabla^2\Phi)\right\}$$
$$+\frac{\beta p}{f_0^3}\frac{\partial}{\partial x}\left(\frac{\partial\Phi}{\partial p}\right)-\frac{R}{c_pf_0^2}\nabla^2Q. \quad (11)$$

As has turned out, it is somewhat advantageous to have the same differential operator operating on the variables $\partial\Phi/\partial t$ and Ω as in Eqs. (10) and (11).

c. Response to diabatic heating

We are interested in studying the response of the Indian atmosphere to diabatic heating Q only. As such, we shall solve the differential equations

$$\left(p^2\frac{\partial^2}{\partial p^2}+2p\frac{\partial}{\partial p}+\frac{\nabla^2}{4k^2}\right)\frac{\partial\Phi}{\partial t}=-\frac{Rp}{c_p}\left(\frac{\partial Q}{\partial p}+\frac{Q}{p}\right) \quad (12)$$

$$\left(p^2\frac{\partial^2}{\partial p^2}+2p\frac{\partial}{\partial p}+\frac{\nabla^2}{4k^2}\right)\Omega=\frac{R}{c_pf_0^2}\nabla^2Q \quad (13)$$

with suitable boundary conditions.

3. Boundary conditions

a. Boundary conditions for $\partial\Phi/\partial t$

We consider infinite extent in the horizontal. For lower boundary conditions, the thermodynamic equation (3) is employed with two assumptions:

(1) convergence of heat due to horizontal advection of temperature is inconsequential compared to *in situ* diabatic heating; and

(2) vertical velocity is due only to frictional pumping in the Ekman layer (Brunt, 1941; Charney and Eliassen, 1949). Hence

$$\left(\frac{\partial}{\partial p}+\frac{C}{p_0T_0}\right)\frac{\partial\Phi_0}{\partial t}=\frac{gC}{p_0T_0}w_f-\frac{R}{p_0c_p}Q_0, \tag{14}$$

where

$$w_f=\mu\nabla^2\Phi_0 \tag{15}$$

$$\mu=(K/2)^{\frac{1}{2}}f_0^{-\frac{3}{2}}\sin 2\alpha_0. \tag{16}$$

K is the eddy diffusivity; α_0 is the angle of inflow near the ground. We treat T_0 as a constant (290 K) at $p=1000$ mb. This is justified due to relatively small variations in the value of T_0. For upper boundary condition, we stipulate that

$$\partial\Phi/\partial t \text{ is finite at } p=0. \tag{17}$$

b. Boundary conditions for Ω

To solve (13), we specify the value of Ω at the lower boundary $p=p_0$

$$\Omega_0=\omega_0/p_0=(\partial\Phi_0/\partial t-g\mu\nabla^2\Phi_0)/RT_0 \tag{18}$$

$$\Omega \text{ finite at } p=0, \tag{19}$$

obtaining $\partial\Phi_0/\partial t$ and $\nabla^2\Phi_0$ from the solution of (12).

4. Solution for $\partial\Phi/\partial t$

We have inhomogeneous differential equation (12) with inhomogeneous boundary conditions (14) and (17). The problem is split up into two component sub-problems:

(1) inhomogeneous differential equation with homogeneous boundary conditions; and
(2) homogeneous differential equation with inhomogeneous boundary conditions.

For sub-problem (1), we visualize forcings from diabatic heating of two Types I and II mentioned in Eq. (1). Each of these heatings is treated separately. In this way, the problem reduces itself to the following:

Let

$$\partial\Phi/\partial t=\partial\Phi_1/\partial t+\partial\Phi_2/\partial t+\partial\Phi_3/\partial t,$$

where $\partial\Phi_1/\partial t$, $\partial\Phi_2/\partial t$, and $\partial\Phi_3/\partial t$ satisfy equations (20), (21), and (22) respectively:

$$\left.\begin{aligned}&\left(p^2\frac{\partial^2}{\partial p^2}+2p\frac{\partial}{\partial p}-\frac{l^2+m^2}{4k^2}\right)\frac{\partial\Phi_1}{\partial t}\\&\quad=-\frac{Q_G}{c_p}R\left\{r\left(\frac{p}{p_0}\right)^r+\frac{p^{r-1}}{p_0{}^r}\right\}e^{i(mx+ly)}\\&\qquad\times\sin\left(\frac{2\pi t}{\Gamma}-\frac{\alpha\pi}{180}\right)\\&\left(\frac{\partial}{\partial p}+\frac{C}{p_0T_0}\right)\frac{\partial\Phi_1}{\partial t}=0 \quad \text{at} \quad p=p_0\\&\frac{\partial\Phi_1}{\partial t}=0 \quad \text{at} \quad p=0\end{aligned}\right\} \tag{20}$$

$$\left.\begin{aligned}&\left(p^2\frac{\partial^2}{\partial p^2}+2p\frac{\partial}{\partial p}-\frac{l^2+m^2}{4k^2}\right)\frac{\partial\Phi_2}{\partial t}\\&\quad=-\frac{Q_H}{c_p}R\left\{8\frac{p}{p_0}-12\left(\frac{p}{p_0}\right)^2\right\}e^{i(mx+ly)}\sin\frac{2\pi t}{\Gamma}\\&\left(\frac{\partial}{\partial p}+\frac{C}{p_0T_0}\right)\frac{\partial\Phi_2}{\partial t}=0 \quad \text{at} \quad p=p_0\\&\frac{\partial\Phi_2}{\partial t}=0 \quad \text{at} \quad p=0\end{aligned}\right\} \tag{21}$$

$$\left.\begin{aligned}&\left(p^2\frac{\partial^2}{\partial p^2}+2p\frac{\partial}{\partial p}-\frac{l^2+m^2}{4k^2}\right)\frac{\partial\Phi_3}{\partial t}=0\\&\left(\frac{\partial}{\partial p}+\frac{C}{p_0T_0}\right)\frac{\partial\Phi_3}{\partial t}=\frac{gC}{p_0T_0}\mu\nabla^2(\Phi_1+\Phi_2+\Phi_3)_{p_0}\\&\qquad-\frac{R}{p_0c_p}Q_Ge^{i(mx+ly)}\sin\left(\frac{2\pi t}{\Gamma}-\frac{\alpha\pi}{180}\right)\\&\partial\Phi_3/\partial t \text{ is finite at } p=0.\end{aligned}\right\} \tag{22}$$

It would be seen that in the lower boundary condition for $\partial\Phi_3/\partial t$, $\nabla^2\Phi_3$ appears on the r.h.s. of (22). Hence it needs special consideration. However, (20), (21), and (22) are linear equations of standard types for which standard methods of solution are available. We applied the method of Green's function. The final solution is given below. Intermediate steps are not given here for economy of space.

$$\frac{\partial\Phi_1}{\partial t}=\frac{Q_G}{c_p}RE_1e^{i(mx+ly)}\sin\left(\frac{2\pi t}{\Gamma}-\frac{\alpha\pi}{180}\right) \tag{23a}$$

$$\Phi_1=-\frac{Q_G}{2\pi c_p}\Gamma RE_1e^{i(mx+ly)}\cos\left(\frac{2\pi t}{\Gamma}-\frac{\alpha\pi}{180}\right) \tag{23b}$$

$$\frac{\partial\Phi_2}{\partial t}=(Q_H/c_p)4RE'e^{i(mx+ly)}\sin(2\pi t/\Gamma) \tag{24a}$$

$$\Phi_2=-(Q_H\Gamma/2\pi c_p)4RE'e^{i(mx+ly)}\cos(2\pi t/\Gamma) \tag{24b}$$

$$\frac{\partial\Phi_3}{\partial t}=-\left(\frac{p}{p_0}\right)^{\nu_1}e^{i(mx+ly)}\frac{2\pi/\Gamma}{\lambda^2+4\pi^2/\Gamma^2}$$
$$\times\left[F_{11}\left\{\frac{2\pi}{\Gamma}\cos\left(\frac{2\pi t}{\Gamma}-\frac{\alpha\pi}{180}\right)-\lambda\sin\left(\frac{2\pi t}{\Gamma}-\frac{\alpha\pi}{180}\right)\right\}\right.$$
$$+F_{12}\{(2\pi/\Gamma)\cos(2\pi t/\Gamma)-\lambda\sin(2\pi t/\Gamma)\}$$
$$\left.+F_2\left\{\lambda\cos\left(\frac{2\pi t}{\Gamma}-\frac{\alpha\pi}{180}\right)+\frac{2\pi}{\Gamma}\sin\left(\frac{2\pi t}{\Gamma}-\frac{\alpha\pi}{180}\right)\right\}\right] \tag{25a}$$

$$\Phi_3=-\left(\frac{p}{p_0}\right)^{\nu_1}\frac{e^{i(mx+ly)}}{\lambda^2+4\pi^2/\Gamma^2}$$
$$\times\left[F_{11}\left\{\frac{2\pi}{\Gamma}\sin\left(\frac{2\pi t}{\Gamma}-\frac{\alpha\pi}{180}\right)+\lambda\cos\left(\frac{2\pi t}{\Gamma}-\frac{\alpha\pi}{180}\right)\right\}\right.$$
$$+F_{12}\{(2\pi/\Gamma)\sin(2\pi t/\Gamma)+\lambda\cos(2\pi t/\Gamma)\}$$
$$\left.+F_2\left\{\lambda\sin\left(\frac{2\pi t}{\Gamma}-\frac{\alpha\pi}{180}\right)-\frac{2\pi t}{\Gamma}\cos\left(\frac{2\pi t}{\Gamma}-\frac{\alpha\pi}{180}\right)\right\}\right] \tag{25b}$$

where ν_1 and ν_2, being roots of $\nu^2+\nu-\pi^2/k^2L^2=0$, are given by

$$\nu_1=-\tfrac{1}{2}+\tfrac{1}{2}(1+4\pi^2/k^2L^2)^{\frac{1}{2}}$$
$$\nu_2=-\tfrac{1}{2}-\tfrac{1}{2}(1+4\pi^2/k^2L^2)^{\frac{1}{2}} \tag{26}$$

$$m^2+l^2=4\pi^2/L^2 \tag{27}$$

$$E_1=\frac{r+1}{(r-\nu_1)(r-\nu_2)(\nu_1+C/T_0)}\{(p/p_0)^{\nu_1}(r+C/T_0)-(p/p_0)^r(\nu_1+C/T_0)\} \tag{28}$$

$$E'=\frac{1}{\nu_1-\nu_2}\left\{\frac{1+\nu_1}{(1-\nu_1)(2-\nu_1)}-\frac{(1+\nu_2)(\nu_2+C/T_0)}{(1-\nu_2)(2-\nu_2)(\nu_1+C/T_0)}\right\}(p/p_0)^{\nu_1}$$
$$+\frac{3}{(2-\nu_1)(2-\nu_2)}(p/p_0)^2-\frac{2}{(1-\nu_1)(1-\nu_2)}(p/p_0) \tag{29}$$

$$\lambda=\frac{gC}{T_0}\frac{\mu}{\nu_1+C/T_0}\frac{4\pi^2}{L^2} \tag{30}$$

$$F_{11}=-\frac{R\lambda}{2\pi/\Gamma}\frac{Q_G}{c_p}\frac{r+1}{r-\nu_2}\frac{1}{\nu_1+C/T_0} \tag{31}$$

$$F_{12}=-\frac{R\lambda}{2\pi/\Gamma}\frac{Q_H}{c_p}\left[\frac{4}{\nu_1-\nu_2}\left\{\frac{1+\nu_1}{(1-\nu_1)(2-\nu_1)}-\frac{1+\nu_2}{(1-\nu_2)(2-\nu_2)}\frac{\nu_2+C/T_0}{\nu_1+C/T_0}\right\}+\frac{12}{(2-\nu_1)(2-\nu_2)}-\frac{8}{(1-\nu_1)(1-\nu_2)}\right] \tag{32}$$

$$F_2=\frac{Q_G}{c_p}\frac{R}{\nu_1+C/T_0}. \tag{33}$$

5. Analysis of the solution $\partial\Phi/\partial t$

It is essential to appreciate the physical significance of various terms occurring in the solution. It is seen from Fig. 1 that for large values of r, e.g., $r=10$, the value of $(p/p_0)^r$ decreases very fast in the lower layers of the atmosphere and practically becomes zero by the 600-mb level; $r=1$ gives a linear decrease from bottom to top of the atmosphere, while $r<1$ gives a slow decrease in the lower layers and fast decrease aloft. Heating of Type I decreases as in the vertical. Large values of r would indicate that heating which had a large vertical gradient at the earth-air interface is unable to penetrate deep into the atmosphere. Diurnal heating would perhaps belong to this class. It is conceivable that diabatic heating which has its source near the ground but which has a period much longer than a day will have correspondingly smaller values for r. For steady state conditions (period $=\infty$), Sankar Rao and Saltzman (1969) felt that r in the neighborhood of 0.75 was most suitable. Murakami's (1967) diabatic heating curve $e^{-7(1-p/p_0)}$ corresponds roughly to $(p/p_0)^6$. Another parameter which enters into the solution is ν_1; e.g., in (25a), vertical variation of $\partial\Phi_3/\partial t$ is given by $(p/p_0)^{\nu_1}$. As seen from (26), ν_1 is always positive; it is a function of L and k. L is the effective wavelength in the horizontal given by (27). For a given value of the static stability parameter C (Eq. 7), k varies directly as the Coriolis parameter (Eq. 8). In this model, k is taken as a constant corresponding to the value of f at 15°N. The variation of ν_1 with L, at latitude 15°N, is shown in Table 1.

Larger wavelengths in the horizontal are associated with relatively smaller values of ν_1. Hence the magnitude of $\partial\Phi_3/\partial t$ is attenuated rapidly in the vertical for

TABLE 1. Variation of ν_1 with L at 15°N.

L (km)	500	1,000	2,000	5,000	10,000	20,000	40,000
ν_1	24.64	12.08	5.80	2.06	0.85	0.30	0.09

relatively short synoptic-scale wavelengths ($L\sim1000$ km), and slowly for planetary-scale wavelengths ($L\sim10{,}000$ km). Now $\partial\Phi_3/\partial t$ is the solution of (22), i.e., of the homogeneous equation with inhomogeneous boundary conditions. In other words, it expresses essentially the influence of forcings near the ground; i.e., according to this solution, the influence of friction in the Ekman layer penetrates more deeply into the atmosphere if the horizontal dimensions of the forcings are large. The influence of horizontal wavelength on the response of the atmosphere has been pointed out by Döös (1961) and Derome and Wiin-Nielson (1971) also.

The influence of friction near the ground on planetary-scale motions is also quite considerable. In order to appreciate the role of this friction, it is worthwhile first to study the solution without friction ($\mu=0$) and then to see how the solution is altered by introduction of friction.

a. Solution without friction

For the frictionless case, we have $\lambda=0$, $F_{11}=0$, $F_{12}=0$; $\partial\Phi_1/\partial t$, Φ_1, $\partial\Phi_2/\partial t$ and Φ_2 remain unaffected, while

$$\frac{\partial\Phi_3}{\partial t}=-(p/p_0)^{\nu_1}e^{i(mx+ly)}\frac{Q_G}{c_p}\frac{R}{\nu_1+C/T_0}\times\sin\left(\frac{2\pi t}{\Gamma}-\frac{\alpha\pi}{180}\right) \quad (34a)$$

$$\Phi_3=(p/p_0)^{\nu_1}e^{i(mx+ly)}\frac{Q_G}{c_p}\frac{R}{\nu_1+C/T_0}\frac{1}{2\pi/\Gamma}\times\cos\left(\frac{2\pi t}{\Gamma}-\frac{\alpha\pi}{180}\right). \quad (34b)$$

1) DIABATIC HEATING OF TYPE I, WITHOUT FRICTION AND WITHOUT DIABATIC HEATING OF TYPE II

In this case, there is only diabatic heating of Type I. We have $0=\mu=\lambda=F_{11}=F_{12}=Q_H=\partial\Phi_2/\partial t=\Phi_2$.

$$\frac{\partial\Phi}{\partial t}=\frac{\partial\Phi_1}{\partial t}+\frac{\partial\Phi_3}{\partial t}=\frac{Q_G}{c_p}REe^{i(mx+ly)}\sin\left(\frac{2\pi t}{\Gamma}-\frac{\alpha\pi}{180}\right) \quad (35a)$$

where

$$E=E_1-\frac{(p/p_0)^{\nu_1}}{\nu_1+C/T_0},$$

and E_1 is defined in (28). Similarly,

$$\Phi=\Phi_1+\Phi_3=-\frac{Q_G}{c_p}REe^{i(mx+ly)}\frac{\Gamma}{2\pi}\cos\left(\frac{2\pi t}{\Gamma}-\frac{\alpha\pi}{180}\right) \quad (35b)$$

E in (35a) and (35b) is a function of r, L, and p. When $r=1.0$, the vertical variation of E for $L=1000$, 5000, 10,000, and 20,000 km is shown in Fig. 2. The following points are noteworthy:

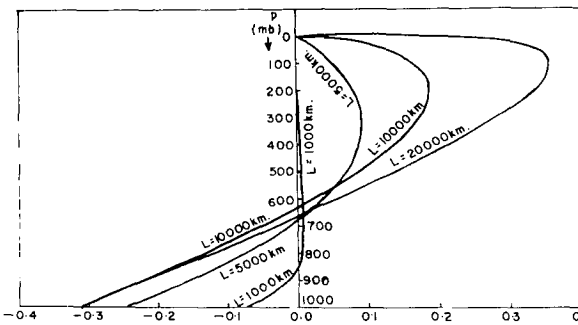

FIG. 2. Variation of E with respect to p for $Q_G/c_p=10^{-6}$ K s^{-1}; $r=1.0$; $L=1000$, 5000, 10,000, and 20,000 km.

i) E is negative in the lower levels and positive aloft, becoming zero at an intermediate level and also at $p=0$; in other words, heating causes a fall of pressure in the lower levels and a rise of pressure aloft. In between, we have a level of phase reversal where $E=0$.

ii) This level of phase reversal first rises with increase of wavelength L from 1000 to 10,000 km but then descends with further increase of L from 10,000 to 20,000 km. It can be shown that, in general, this level of phase reversal p_r is given by

$$\frac{p_r}{p_0}=(\nu_1+C/T_0)\Big/\left\{\frac{\pi^2}{k^2L^2(r+1)}+C/T_0\right\}. \quad (36)$$

Figure 3 shows how the level of phase reversal changes with r and L. It highlights the following features:

a) For a given value of L, the level of phase reversal rises as r decreases.
b) For any given value of r, there is a wavelength for which the level of phase reversal is at a maximum distance above the ground.

iii) In Fig. 2, the level of maximum E is seen to rise with increase of wavelength. For $L=1000$ km, this level is close to 650 mb. For wavelengths of 5000, 10,000, and 20,000 km, this level of maximum E is close to 300, 200, and 100 mb respectively.

iv) It can be shown that in general p_x, the level of maximum E, is given by

$$\frac{p_x}{p_0}=(r/\nu_1)^{1/\nu_1-r}\frac{p_r}{p_0}. \quad (37)$$

The variation of this level with r and L is shown in Fig. 4. The following features are noteworthy.

a) As r decreases, the height of maximum E increases.
b) As L increases, the height of maximum E increases.

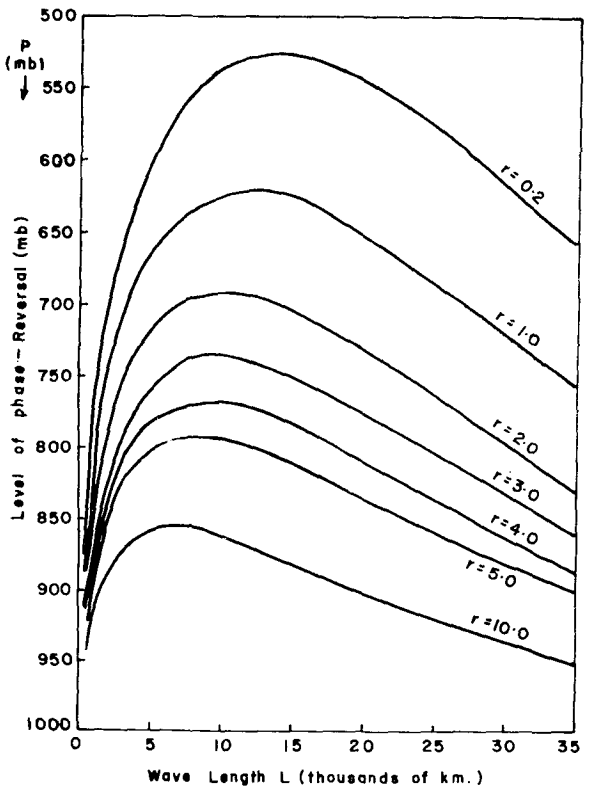

FIG. 3. Level of phase reversal as a function of r and L.

c) For $r=0.2$, even a wavelength of 5000 km will have the level of maximum E as high as 150 mb; whereas for $r=5.0$, the level of maximum E will always be below the 400-mb level for all wavelengths physically possible on the earth's surface.

d) If there is a wind variation essentially due to diabatic heating oscillation, the maximum variation in wind will occur at the level of maximum E. This variation may manifest itself in the form of strong wind, its level depending on the vertical profile of diabatic heating and also on the horizontal extent of the heating. It would be interesting to study some of the known low-level and high-level jet streams in the atmosphere from this point of view.

v) A practical analyst or forecaster would like to have a quick method of estimating height tendency for various vertical distributions of diabatic heating of Type I. Figure 2 can serve that purpose when $r=1.0$. From (35a), the amplitude of height tendency at any level is given by

$$(\partial z/\partial t)_{\text{amplitude}}=(Q_G/c_p)(RE/g). \tag{38}$$

Here, Q_G/c_p is temperature tendency at the ground due to diabatic heating; R/g is the reciprocal of the autoconvective lapse rate and is equal to 29.29 m·K^{-1}. If $Q_G/c_p=1$ K d^{-1}, then

$$(\partial z/\partial t)_{\text{amplitude}}=29.29E \text{ m}\cdot\text{d}^{-1}. \tag{39}$$

E can be approximately read from Fig. 2 and a quick estimate of height tendency made straightaway.

2) DIABATIC HEATING OF TYPE II WITHOUT FRICTION AND WITHOUT DIABATIC HEATING OF TYPE I

In this case, $\mu=0$, $Q_G=0$, $Q_H\neq 0$.

$$0=\lambda=F_{11}=F_{12};\ \partial\Phi_1/\partial t=0=\Phi_1.$$
$$F_2=0;\ \partial\Phi_3/\partial t=0=\Phi_3.$$

We have a trivial solution for Eq. (22).

$$\therefore\quad \frac{\partial\Phi}{\partial t}=\frac{\partial\Phi_2}{\partial t}=\frac{Q_H}{c_p}=4RE'e^{i(mx+ly)}\sin 2\pi t/\Gamma \tag{40a}$$

$$\Phi=\Phi_2=-(Q_H/c_p)(\Gamma/2\pi)4RE'e^{i(mx+ly)}\times\cos 2\pi t/\Gamma. \tag{40b}$$

E' is analogous to E. It is a function of L and p. Variation of E' with p is shown in Fig. 5 for $L=1000$, 5000, 10,000, and 20,000 km. The following points are noteworthy:

a) E' is negative in the lower layers and positive aloft, becoming zero at $p=0$.

b) The level of the upper-level maximum rises as wavelength increases. The maximum occurs around 200 mb when $L=5000$ km, around 125 mb when $L=10{,}000$ km, and around 100 mb when $L=20{,}000$ km.

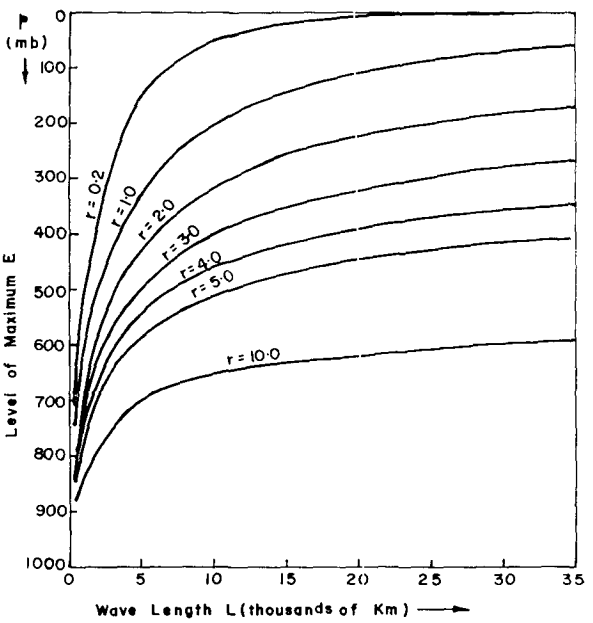

FIG. 4. Level of maximum E as a function of r and L.

c) The magnitude of the upper-level maximum also increases with wavelength. For $L=20{,}000$ km, the magnitude is about twice that for $L=10{,}000$ km and about four times that for $L=5000$ km.
d) For a given value of L, the level of phase reversal in case of heating of Type II is higher than for heating of Type I with $r \gtrsim 1.0$.
e) If diabatic heating of Type II corresponds to 1.0 K day^{-1} at the 500-mb level, then the height tendency at any level is given by

$$\partial z/\partial t = 29.29E' e^{i(mx+ly)} \sin 2\pi t/\Gamma. \quad (41)$$

The value of E' can be easily read from Fig. 5. For example, for $L=10{,}000$ km we have $E'=0.41$ at the 125 mb level. Therefore $(\partial z/\partial t)_{\text{amp}} \sim 12$ m·d^{-1} at the 125-mb level; phase reversal in this case takes place near the 510-mb level.

b. Solution with friction

1) HEATING OF TYPE I+GROUND FRICTION ($Q_H=0$; $Q_G\neq 0$; $\mu\neq 0$)

Substituting in (23) to (25), we get

$$0 = \partial\Phi_2/\partial t = \Phi_2$$

$$\Phi=\Phi_1+\Phi_3=-\frac{Q_G}{c_p}\frac{R}{\nu_1+C/T_0}e^{i(mx+ly)} \times A\cos\left(\frac{2\pi t}{\Gamma}-\alpha-\epsilon\right)$$

$$A\sin\epsilon=(p/p_0)^{\nu_1}\frac{1}{\lambda^2+4\pi^2/\Gamma}\frac{\nu_1\lambda}{r-\nu_2} \quad (42a)$$

$$A\cos\epsilon=-\frac{1}{2\pi/\Gamma}\left[\frac{r+1}{(r-\nu_1)(r-\nu_2)} \times\{(p/p_0)^r(\nu_1+C/T_0)-(p/p_0)^{\nu_1}(r+C/T_0)\} +(p/p_0)^{\nu_1}\frac{1}{\lambda^2+4\pi^2/\Gamma^2}\{(4\pi^2/\Gamma^2) +\lambda^2(r+1)/(r-\nu_2)\}\right]. \quad (42b)$$

Comparing this solution with (35b), which is the corresponding solution without friction, one finds that low-level friction:

a) reduces the intensity of pressure deficit in the lower layers and enhances the pressure excess aloft;
b) brings down the level of phase reversal; and
c) creates a phase difference in the pressure wave at various levels. In general, extreme low pressure in the lower layers occurs before the extreme high pressure aloft.

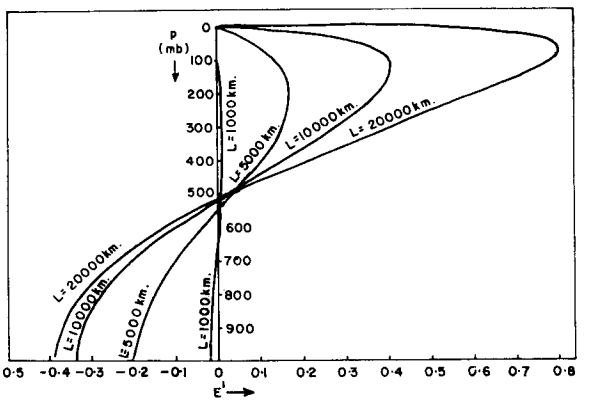

FIG. 5. Variation of E' with respect to p for $Q_H/c_p=10^{-6}$ K s^{-1}; $L=1000$, 5000, 10,000, and 20,000 km.

Points (a) and (b) are brought out clearly in Fig. 6. This shows the amplitude of geopotential oscillation at various levels for different values of friction coefficient ($\mu=0.0$, 0.2, 0.4, 0.6, 0.8, and 1.0 in units of 10^6 m·s); $L=13{,}500$ km and $\mu=0$ represents the frictionless case discussed in Section 5a (1) $Q_G/c_p=1.0\times10^{-6}$ K s^{-1}; $\Gamma=1$ year.

Point (c) regarding phase lag is illustrated in Fig. 7 (a–f). Here, the amplitude and phase of the geopotential wave at specified isobaric levels is vectorially represented for different values of frictional coefficient μ. The phase of the maximum in the heat wave at all levels is represented by the x-axis. Vectors represent the amplitude and phase of the maximum in the geopotential wave.

In Fig. 7a, the dots are the ends of the vectors representing the amplitude and phase of pressure wave at various levels for the frictionless case, $\mu=0$. The

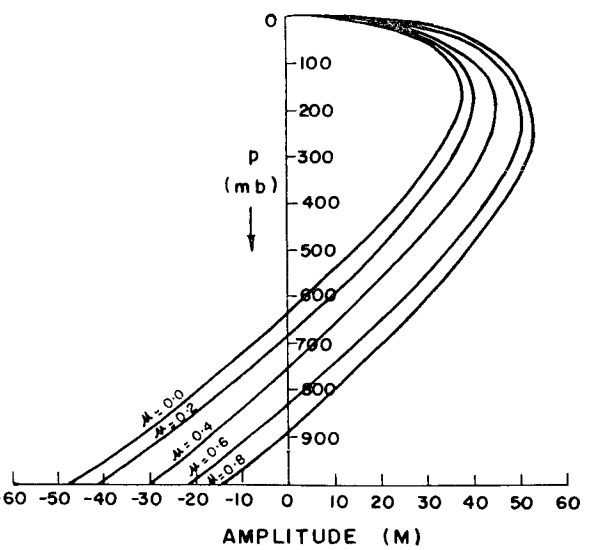

FIG. 6. Amplitude of Z (m) for annual oscillation with different values of μ; $L=13{,}500$ km, $\alpha=0$, $Q_G/c_p=10^{-6}$ K s^{-1}.

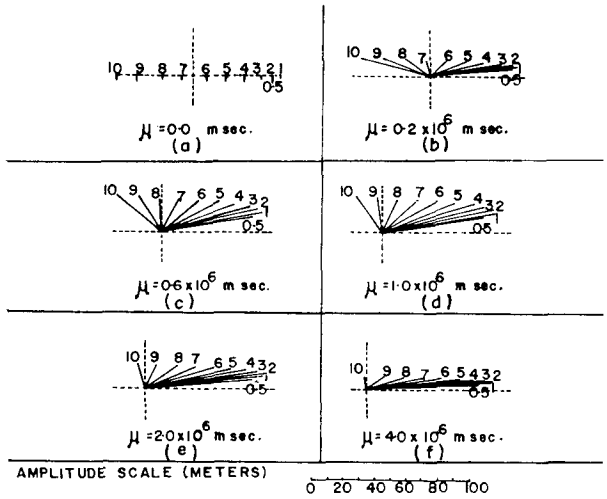

FIG. 7. Amplitude-phase diagram for annual wave at different constant pressure levels. Horizontal wavelength=20,000 km; amplitude in meters; pressure in decibars. Heating of Type I only; $r=1.0$; $Q_G/c_p=10^{-6}$ K s^{-1}.

numerals near dots represent the value of pressure in decibars. Thus, the *height wave* at the 1000-mb level has the amplitude of 48.7 m and the phase of its maximum is 180° when the phase of maximum in *heat wave* is 0°. Thus the phase of the geopotential wave at all levels below 700 mb is 180° different from that of the heat wave but the geopotential wave is exactly in phase with the heat wave at all levels above 600 mb. There is a phase reversal in the geopotential wave between 600 and 700 mb; i.e., when there is a crest in the diabatic heat wave, there is a trough in the geopotential wave at all levels below 620 mb and a crest at all levels above 620 mb.

Analysis showed that as μ increases from 0.0 to 0.5 $\times 10^6$ m·s, the vectors corresponding to the lower troposphere continuously rotate in a clockwise direction and the vectors corresponding to the higher layers rotate counter-clockwise. At $\mu \geqslant 0.6\times 10^6$ m·s, the vectors at all levels rotate clockwise. We have not investigated the significance of this value of μ. For very large values of $\mu(\geqslant 10^7$ m·s) the height wave, at all levels except near the ground, comes to be closely in phase with the diabatic heat wave, whereas the height wave at the ground has a lag of nearly 90° behind the diabatic heat wave. In other words, for very large values of μ, the low pressure wave near the ground is ahead of the high pressure wave aloft by about a quarter period of the heat wave.

In Fig. 7b, the continuous lines are the vectors representing the amplitude and phase of height crest at different constant pressure levels for $\mu=0.2\times 10^6$ m·s. By rotating these vectors through 180°, we get vectors representing height troughs. Figures 7(c–f) show corresponding features when $\mu=(0.6, 1.0, 2.0, 4.0)\times 10^6$ m·s, respectively.

2) HEATING OF TYPE II+GROUND FRICTION ($Q_G=0$; $Q_H\neq 0$; $\mu\neq 0$)

Substituting in (23) to (25), we get

$$\Phi=\Phi_2+\Phi_3=-(Q_H/c_p)4Fe^{i(mx+ly)}\times A'\cos(2\pi t/\Gamma-\epsilon')$$

$$A'\sin\epsilon'=-(p/p_0)^{\nu_1}\frac{\lambda^2}{\lambda^2+4\pi^2/\Gamma^2}\left[\frac{1}{\nu_1-\nu_2}\left\{\frac{1+\nu_1}{(1-\nu_1)(2-\nu_1)}-\frac{(1+\nu_2)(\nu_2+C/T_0)}{(1-\nu_2)(2-\nu_2)(\nu_1+C/T_0)}\right\}+\frac{3}{(2-\nu_1)(2-\nu_2)}-\frac{2}{(1-\nu_1)(1-\nu_2)}\right] \quad (43a)$$

$$A'\cos\epsilon'=\frac{\Gamma}{2\pi}\left[(p/p_0)^{\nu_1}\frac{4\pi^2/\Gamma^2}{(\nu_1-\nu_2)(\lambda^2+4\pi^2/\Gamma^2)}\left\{\frac{1+\nu_1}{(1-\nu_1)(2-\nu_1)}-\frac{(1+\nu_2)(\nu_2+C/T_0)}{(1-\nu_2)(2-\nu_2)(\nu_1+C/T_0)}\right\}-\frac{3}{(2-\nu_1)(2-\nu_2)}\right.$$
$$\times\left\{(p/p_0)^{\nu_1}\frac{\lambda^2}{\lambda^2+4\pi^2/\Gamma^2}-(p/p_0)^2\right\}+\frac{2}{(1-\nu_1)(1-\nu_2)}$$
$$\left.\times\left\{(p/p_0)^{\nu_1}\frac{\lambda^2}{\lambda^2+4\pi^2/\Gamma^2}-p/p_0\right\}\right]. \quad (43b)$$

This solution with different values of μ has been compared with that which was obtained without friction in section 5a (2). Qualitatively, friction has the same effect as stated in section 5b (1) in case of heating of Type I. The vectors representing the amplitude and phase of height crest at different constant pressure

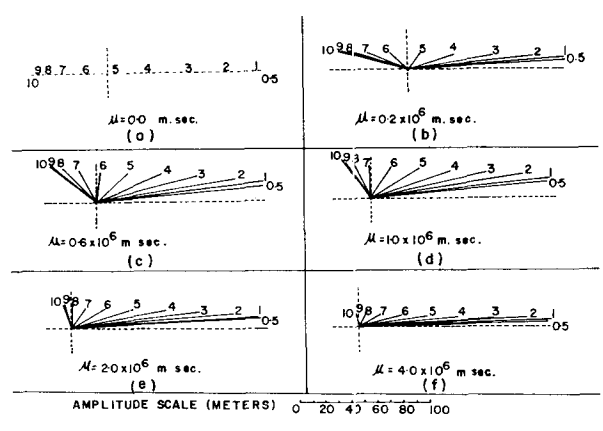

FIG. 8. As in Fig. 7, except for heating of Type II only; $Q_H/c_p=10^{-6}$ K s^{-1}.

levels for different values of frictional coefficient μ are shown in Figs. 8(a–f).

3) HEATING OF TYPES I AND II+GROUND FRICTION

Figures 7 and 8 give the amplitude of the wave and the phase of the ridge line when Q_G/c_p and Q_H/c_p are each equal to 10^{-6} K s^{-1}. To get the combined influence of b_1 units of heating of Type I and b_2 units of heating of Type II, we have to take b_1 times the vectors given in Fig. 7 and b_2 times the vectors given in Fig. 8 and add these vectorially. The resultant vectors would represent the amplitude of the total height wave and the phase of the ridge line at different levels.

Part II: Application to the Indian Monsoon oscillation

6. Parameters of the model for monsoonal oscillation

The analysis presented in Sections 2 to 5 indicated a clear possibility that some of the known features of the 12-monthly oscillation of the monsoon over the Northern Hemisphere in general and over India in particular could be simulated through this model. The observed features of the 12-monthly oscillation as relevant to this model are presented below:

i) Undoubtedly, there are asymmetries along a latitude circle. Nevertheless, there is also an element of symmetry along a latitude circle, particularly in the middle and upper troposphere. Hence, in the first instance, we could take $m=0$ in $e^{i(mx+ly)}$ of the model and consider time variations in the y,p plane only.

ii) In the y-direction, the amplitude of the observed oscillation is nearly zero at the equator and highest in the middle and higher latitudes. For the purpose of a plane cartesian coordinate system, one could consider the distance from equator to 45°N as roughly a quarter wavelength; i.e., $L\sim 20{,}000$ km.

iii) In the vertical, observations show a phase reversal in the lower troposphere. Aloft, the maximum amplitude occurs in the upper troposphere or in the lower stratosphere. This suggested that the results obtained in Sections 2 to 5 for L in the range of 15,000 to 20,000 km would fit pretty well with the observations. We adopted $L=20{,}000$ km.

iv) The amplitude of the observed low pressure wave in the lower troposphere is considerably less than that of the high pressure wave in the upper troposphere. Further, observations show a phase lag between the lower-level and upper-level waves in qualitative agreement with the theoretical solution with friction discussed in section 5b above. Hence, introduction of low-level friction in the model was considered essential. The necessity of low-level friction in the theory of planetary scale circulations has been amply demonstrated by previous studies (Charney and Eliassen, 1949; Smagorinsky, 1953, 1963; Philips, 1956; Brown, 1964; Mintz and Arakawa, 1965; Leith and Manabe, 1971; Delsol, Miyakoda, and Clarke, 1971; Everson and Davies, 1972; Webster, 1972).

For assigning a value to the frictional coefficient μ in (15), we examined the amplitude and phase of the annual atmospheric pressure oscillation at various levels and compared the same quantitatively with the solution (with friction) presented in Section 5b (Figs. 7 and 8). It was found that $\mu=0.6\times10^6$ m·s would be appropriate provided that this value be also acceptable on the basis of friction-layer theory.

While we found that we could easily adopt the formulation of friction as given by Charney and Eliassen (1949), we could not straightaway adopt their value of K, the coefficient of diffusivity. For their value of $K=10$ m^2 s^{-1} and $\alpha_0=\pi/8$, we would have $\mu=4.5\times10^6$ m·s and Z_E, the top of Ekman layer, at 1.74 km when $f=0.5\times10^{-4}$ s^{-1}. This value of Z_E is rather too high. Review of the literature shows that there is considerable scope for varying the effective value of K in the theory of the Ekman layer. For example, Ekman-layer theory assumes K to be constant in the vertical. This has been seriously questioned by Rossby and Montgomery (1935) and by Pasquill (1962, p. 76). The former thought that K is nearly zero above 0.5 km or so. Even at a given level (2 m), for a given wind speed (5 m s^{-1}), the values of K given by Pasquill (1962, p. 72) varies from 0.13 m^2 s^{-1} over mud flats to 0.56 m^2 s^{-1} over fully grown crops. Between day and night, K is known to vary by a factor of 12 (Haltiner and Martin, 1957, p. 242). Further, the atmosphere is neither barotropic nor in steady state as assumed in the development of Eqs. (15) and (16).

We found that $K=4$ m^2 s^{-1} and $Z_E=0.97$ km for $f=0.5\times10^{-4}$ s^{-1} at 20°N yields $\mu=0.6\times10^{-6}$ m·s, the value adopted in our computations. This appears to lie within the acceptable range of values.

v) Considerable effort was put into determining plausible values of diabatic heating parameters of the model, namely Q_G/c_p, Q_H/c_p, r, α, time of the year corresponding to $t=0$ and the latitude corresponding to $y=0$. It is well known that we do not have a direct method of measuring the diabatic heating distribution in the atmosphere. It has had to be determined indirectly. Attempts made to determine the diabatic heating distribution indirectly can be grouped in three broad categories:

a) from the prognostic form of thermodynamic Eq. (3) (Brown, 1964; Reed and Recker, 1971);
b) from the diagnostic (steady state) form of (3) (Smagorinsky, 1953; Murakami, 1957a, b; Academia Sinica, 1958; Döös, 1962; Asakura and Katayama, 1964; Saltzman, 1965; Sankar Rao and Saltzman, 1969); and
c) by inclusion of physical laws of heat exchanges in numerical models of the general circulation and extracting information about Q from the history

tapes of computation (Manabe, Smagorinsky, and Strickler, 1965).

From these studies, one can derive the following two conclusions:

a) It is quite reasonable to assume two types of vertical variation of Q as given by Eq. (1).

b) Magnitude of diabatic heating depends on the space and time scales of the meteorological phenomenon. For synoptic weather systems, amplitude of the heating function is of the order of 10 K d^{-1} (Reed and Recker, 1971; Murakami, 1972). For quasi-steady, planetary-scale systems, it is of the order of 2 K d^{-1} (Manabe, Smagorinsky, and Strickler, 1965). For planetary-scale, annually oscillating systems, a much smaller value of the order of 0.2 K d^{-1} would be adequate (Dickinson, 1971). Observations also show that the heat content of the atmosphere over Asia is nearly at a maximum during July and a minimum during January. In our model, the heat content due to heating of Type II would also be at maximum during July and minimum during January if $t=0$ in Eq. (1) corresponds to some date in January. By trial, it was found that $t=0$ corresponding to 5 January was suitable. It also became clear that the amplitude of heating of Type II was to be larger than that of Type I. A phase difference in the heating along the vertical was to be provided through α. After a close inspection of the influences of various heating parameters separately, we decided upon the following values:

$$Q_G/c_p=10^{-6}\ \text{K s}^{-1};\ Q_H/c_p=2.5\times10^{-6}\ \text{K s}^{-1};\quad r=1;\ \alpha=90°. \tag{44}$$

Type I heating corresponds to a maximum heating rate of 0.086 K d^{-1} at 1000 mb, linearly decreasing to zero at the top of the atmosphere, $p=0$. Type II gives a heating rate of 0.215 K d^{-1} at 500 mb, parabolically decreasing to zero at the bottom and top of the atmosphere.

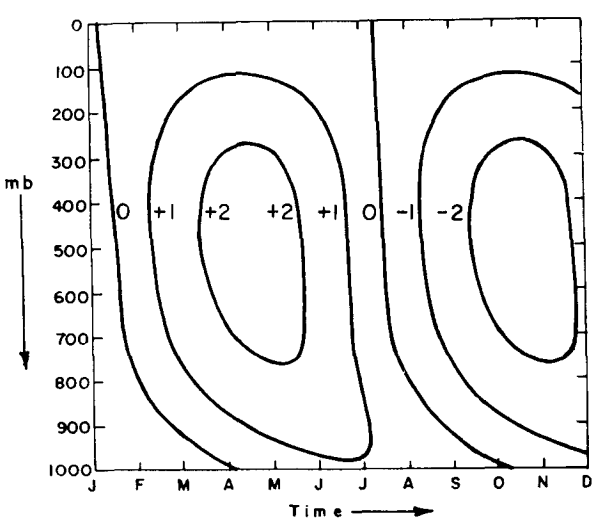

FIG. 9. The quantity $(p/p_0)\{10(1-p/p_0)\sin2\pi t/\Gamma-\cos2\pi t/\Gamma\}$ of Eq. (45) showing distribution of time-rate of diabatic heating.

The time rate of diabatic heating (Q_1+Q_2) at any point (y,p) at time t is given by

$$(Q_1+Q_2)/c_p=10^{-6}\sin\frac{2\pi y}{L}\left[\frac{p}{p_0}\{10(1-p/p_0)\sin2\pi t/\Gamma-\cos2\pi t/\Gamma\}\right]. \tag{45}$$

The distribution of

$$(p/p_0)\{10(1-p/p_0)\sin2\pi t/\Gamma-\cos2\pi t/\Gamma\}$$

in height and time is shown in Fig. 9. Points on the abscissa indicate the first days of the months January, February, etc. The ordinate denotes the vertical p-coordinate. From the isopleths, it is seen that as a result of these two types of heating, there is a maximum rate of diabatic heating in the middle troposphere during April–May and maximum diabatic cooling during October–November, with considerable phase shift along the vertical in the lower troposphere.

The total diabatic heat (H_1+H_2) absorbed by the atmosphere per gram of air from time $t=0$ (5 January) to any time t is given by

$$H_1+H_2=\int_0^t(Q_1+Q_2)dt=\frac{\Gamma c_p}{2\pi}\sin\frac{2\pi y}{L}10^{-6}[(p/p_0)\times\{10(1-p/p_0)(1-\cos2\pi t/\Gamma)-\sin2\pi t/\Gamma\}]. \tag{46}$$

The distribution of

$$(p/p_0)\{10(1-p/p_0)(1-\cos2\pi t/\Gamma)-\sin2\pi t/\Gamma\}$$

in height and time is shown in Fig. 10. Here also, the abscissa indicates the first day of the months January, February, etc. It is seen that with reference to the fifth day of January at all levels, the total of diabatic heat absorbed by the atmosphere is positive over most of the region except in the lowest layers of the troposphere during the early part of the year. Maximum absorption occurs in the middle troposphere during mid-July with a marked phase shift in the lower troposphere. Figures 9 and 10 also indicate that the mid-tropospheric heating (Type II) is the dominant part of the prescribed diabatic heating in this model and that Type I heating largely acts to provide a phase shift of heating in the vertical.

In the Indian monsoon region around longitude 77.5°E, we have essentially the Indian Ocean south of latitude 5°N and a land region to its north. Observations show that the amplitude of the annual oscillation of pressure and temperature in the near-equatorial oceanic region is nearly zero. Hence we took $y=0$ at 5°N.

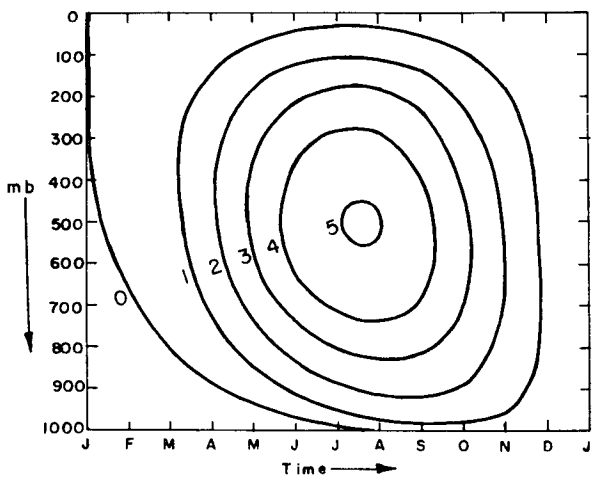

FIG. 10. The quantity $(p/p_0)\{10(1-p/p_0)(1-\cos 2\pi t/\Gamma) - \sin 2\pi t/\Gamma\}$ of Eq. (46) showing distribution of total diabatic heat absorbed since $t=0$.

7. Results of the model

a. Zonal motion

With the parameters given in Section 6 above, we computed the pressure, temperature, zonal wind, and vertical velocity corresponding to the annual oscillation along meridian 77.5°E between latitudes 5°N and 50°N. From observations, we know the year's average distribution of pressure, temperature, and zonal wind with a fair degree of accuracy. Taking this observed annual average picture as given, we added to it the components of the computed annual oscillation and got the resulting picture at various times of the year. The picture of such computed zonal wind (observed annual mean+computed oscillation wind) in the middle of four representative months (January, April, July, and October) between latitudes 5°N and 35°N is presented in Fig. 11(a–d). For comparison, we present in Fig. 12(a–d) the observed normal zonal wind during the same months along 77.5°E. North of 31°N along 77.5°E, there are the Himalayan mountains. To complete Fig. 12 north of 31°N, we have utilized winds observed at neighboring low-level stations a few degrees to the west of 77.5°E.

By and large, the zonal winds in the upper troposphere are simulated pretty well. Thus, the model is able to reproduce the westerly jet stream over north India during winter (January) and the easterly jet stream over south India during summer (July). The positions of the jet cores in respect of both latitude and height are given correctly by the model. However, the model underestimates the strength of the westerly jet stream in winter, giving a maximum speed between 30 and 35 m s^{-1} whereas the actual maximum speed is between 40 and 45 m s^{-1}. The strength of the easterly jet stream during summer is, however, simulated cor-

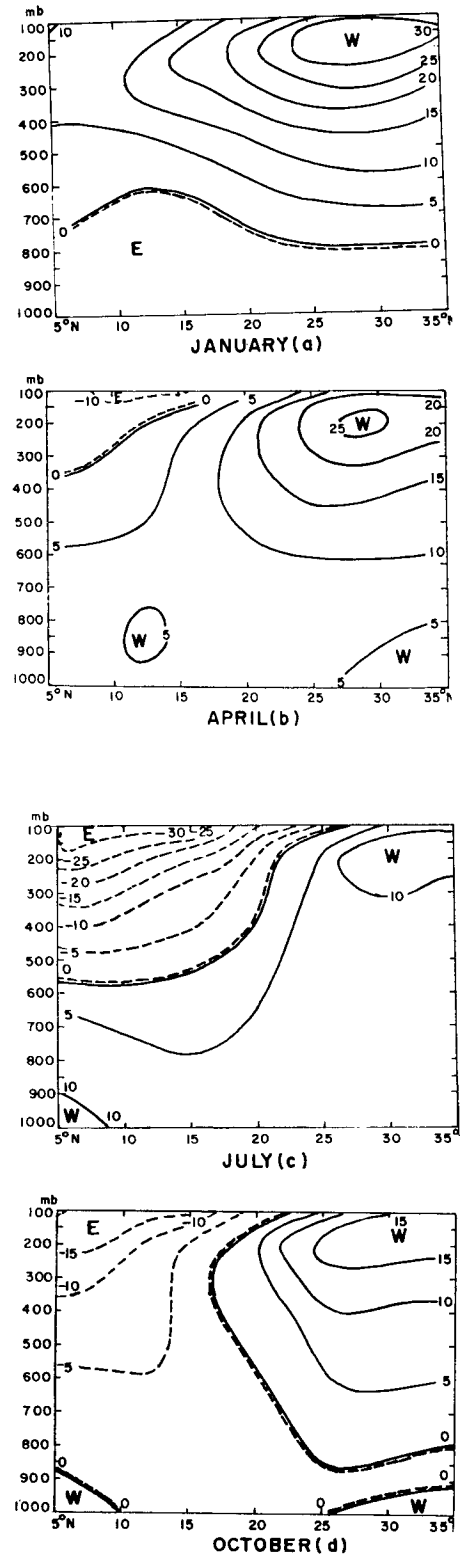

FIG. 11. Vertical cross section of zonal wind (m s^{-1}) along 77.5°E between 5°N and 35°N (model) for the months of (a) January; (b) April; (c) July; and (d) October.

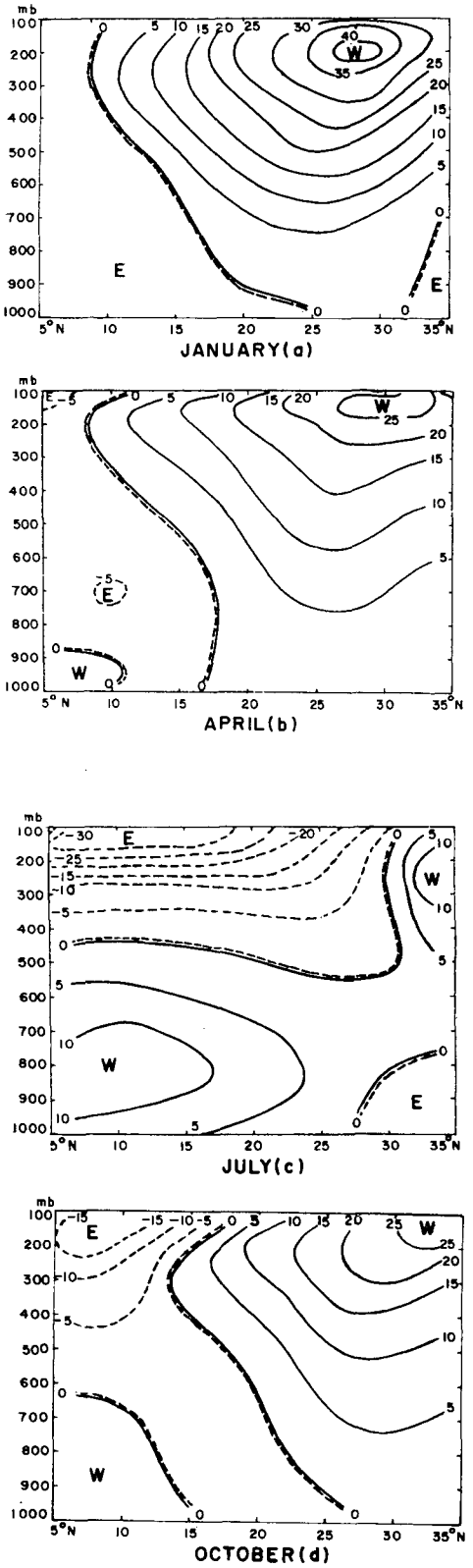

FIG. 12. As in Fig. 11, for observed winds.

rectly (between 30 and 35 m s^{-1}) by the model. Even in the transition months—April and October—the zonal winds in the upper troposphere are simulated well.

In July when there are easterlies aloft, the model is able to reproduce well the low-level westerlies south of 20°N, but the observed weak lower-tropospheric easterlies north of 27°N are not reproduced.

From April to July, the upper-tropospheric easterlies south of the Indian region progressively spread downwards as well as northwards, with the axis of maximum easterly wind tilting upward towards south in the actual situation as well as in the model. From summer to winter, the easterly regime loses its hold and the westerlies invade nearly the whole country in the middle and the upper troposphere. This is brought out well by the model.

On the whole this model, which is extremely simple and almost crude, with one wavelength in the y-direction and with one period in time, is able to reproduce quite a few of the main features of the observed zonal wind oscillation in the Indian region throughout the year. The purpose of this experimental computation, with these elementary prescriptions, was not to explain all the observed features of the zonal wind oscillation throughout the year, but to test and see how much can be explained with the minimum number of parameters.

The model has several limitations. We have not explained how the annual mean pattern is maintained, nor have we explained the physical mechanism for the heating function given in Eq. (1). We have also neglected all the advective effects, including the β-effect as well as the north-south eddy transports of heat and momentum. These advective effects are known to be important for the maintenance of the annual mean circulation as well as for the index cycle of the atmosphere. Presumably, these advective effects are important for the annual oscillation as well. In spite of these limitations of the model, there is quite good agreement with the real atmosphere; the values of Q also seem reasonable. It is therefore conceivable that the forcing we prescribed through the term

$$\frac{Rp}{c_p}\left(\frac{\partial Q}{\partial p}+\frac{Q}{p}\right)$$

on the r.h.s. of (10) implicitly includes the net effect also of the advective terms on the same side of the equation, although it appears that advection has been completely neglected; or it may be that in the monsoon region, the net effect of advection is very important for the maintenance of the annual mean circulation but not too important for forcing the annual oscillation. In any case, we admit that ours is not a comprehensive model and a lot more work remains to be done to understand the monsoon circulation quantitatively in

terms of simple analytical forcing functions.

b. Vertical motion

Vertical velocity $\omega \equiv dp/dt$ associated with the annual oscillation is given by

$$\omega = \omega_{11}+\omega_{12}+\omega_{13}+\omega_{21}+\omega_{22}+\omega_{23}+\omega_{32}+\omega_{33} \tag{47}$$

$$\omega_{11} = \frac{Q_G}{c_p}\frac{\pi^2}{k^2L^2}\frac{1}{(r-\nu_1)(r-\nu_2)}\frac{\rho_0 R}{C/T_0}\{(p/p_0)^{r+1}-(p/p_0)^{-\nu_2}\} \times \sin\frac{2\pi y}{L}\sin\left(\frac{2\pi t}{\Gamma}-\frac{\alpha\pi}{180}\right) \tag{48}$$

$$\omega_{12} = \rho_0(\partial\Phi_1/\partial t)_{p=p_0}(p/p_0)^{-\nu_2} \tag{49}$$

$$\omega_{13} \doteqdot -g\rho_0\mu(\nabla^2\Phi_1)_{p_0}(p/p_0)^{-\nu_2} \tag{50}$$

$$\omega_{21} = \frac{Q_H}{c_p}\frac{\pi^2}{k^2L^2}\frac{4\rho_0 R}{C/T_0}\left[\frac{1}{(1-\nu_1)(1-\nu_2)}\{(p/p_0)^2-(p/p_0)^{-\nu_2}\} - \frac{1}{(2-\nu_1)(2-\nu_2)}\{(p/p_0)^3-(p/p_0)^{-\nu_2}\}\right] \times \sin\frac{2\pi y}{L}\sin\frac{2\pi t}{\Gamma} \tag{51}$$

$$\omega_{22} = \rho_0(\partial\Phi_2/\partial t)_{p_0}(p/p_0)^{-\nu_2} \tag{52}$$

$$\omega_{23} \doteqdot -g\rho_0\mu(\nabla^2\Phi_2)_{p_0}(p/p_0)^{-\nu_2} \tag{53}$$

$$\omega_{32} = \rho_0(\partial\Phi_3/\partial t)_{p_0}(p/p_0)^{-\nu_2} \tag{54}$$

$$\omega_{33} \doteqdot -g\rho_0\mu(\nabla^2\Phi_3)_{p_0}(p/p_0)^{-\nu_2}. \tag{55}$$

By and large, the terms ω_{13}, ω_{23}, and ω_{33} containing the frictional term μ are the most important terms in respect of magnitude; ω is negative and hence w is positive in the region where we have positive relative vorticity near the ground. Φ_1, Φ_2 and Φ_3 are given by (23b), (24b), and (25b), respectively. Strictly speaking, vertical velocity due to friction should be taken as zero at $p=p_0$; it should increase to a maximum value at the top of Ekman layer $p=p_f$ and then decrease upwards as $(p/p_f)^{-\nu_2}$. However, in formulae (50), (53), and (55), p_f has been replaced by p_0 as an approximation. This is tolerable to the extent that application of Ekman-layer theory to the present case is itself a big approximation, because the layer in question is neither barotropic nor in steady state as required for strict application of Ekman-layer theory. Accepting this as an approximate theory, it is seen that the vertical velocity induced by friction decreases as $(p/p_0)^{-\nu_2}$. In Table 1, we have the values of ν_1 which is always positive. Since $1+\nu_1=-\nu_2$ and $(p/p_0)^r$ is sketched in Fig. 1, it is easy to appreciate how fast the vertical velocity induced by friction is attenuated upwards for synoptic-scale disturbances ($L\sim 1000$ km), while it decreases rather slowly and penetrates more deeply into the atmosphere for planetary-scale disturbances ($L\sim 10{,}000$ km). Corresponding to $L=20{,}000$ km as in our case, the vertical velocity above the frictional layer decreases upwards as $(p/p_0)^{1.3}$. Further,

$$\omega_{13}+\omega_{23}+\omega_{33} = -g\rho_0\mu(\nabla^2\Phi_1+\nabla^2\Phi_2+\nabla^2\Phi_3)_{p_0}(p/p_0)^{\nu'+1}. \tag{56}$$

Since $\nabla^2=-4\pi^2/L^2$, it follows that ω_f induced by friction is in phase with $(\Phi_1+\Phi_2+\Phi_3)$. When the sea-level pressure is less than the annual mean, as happens during summer, ω_f is negative and the vertical motion is upwards. The reverse downward motion occurs during winter.

8. Conclusions

1) Until satisfactory methods become available for measuring diabatic heating distributions in space and time, hypothetical heating functions of the types given in Eq. (1) and the methodology followed in this paper are useful for estimating diabatic heating and its influence in the atmosphere.

2) The horizontal extent of heating and cooling is very important. Planetary-scale wavelengths have their maximum pressure effect close to jet-stream level near the tropopause. Vertical motions induced by low-level friction also penetrate to great heights if the horizontal extent of heating is large.

3) Diabatic heating coupled with low-level friction seems to determine some of the major features of the annual monsoonal circulation over the Indian region. Quantitative agreement comes out to be very satisfactory.

4) Vertical motion induced by diabatic heating and low-level friction is of the direct circulation type, i.e., warmer air rises and cooler air sinks.

5) It is surprising that such a simple and almost crude quasi-geostrophic model is able to explain quantitatively some of the major observed features of annual monsoonal oscillation.

6) Improvement of the model requires additional work:

a) to explain the dynamics of the steady-state pattern which has been assumed in this paper;
b) to explain the physics behind the assumed distributions of diabatic heating in space and time;
c) to introduce variations in the x-direction also; and
d) to consider the effects of advection.

Acknowledgments. The authors are grateful to their colleagues Dr. R. N. Keshavamurty and Dr. R. Ananthakrishnan for valuable discussions, to Mr. Pathan and Mrs. George for several computations, and to the Drawing Branch of the Institute for the figures presented in this paper.

REFERENCES

Academia Sinica, 1958: On the general circulation over eastern Asia. *Tellus*, **10**, 299–312.

Asakura, T., and A. Katayama, 1964: Normal distribution of heat sources and sinks in lower troposphere over northern hemisphere. *J. Meteor. Soc. Japan*, **42**, 209–244.

Asnani, G. C., and A. U. Rao, 1963: Seasonal changes in the circulation pattern over India and Neighbourhood. *Proc. Symp. on Tropical Meteor.* (J. W. Hutchings, ed.) Rotorua, New Zealand, 207–215.

Böhme, W., 1954a: Über thermisch bedingte Zirkulationsmechanismenin einerim Grundzustand rahenden, isothermen atmosphäre. *Z. Meteor.*, **8**, 52–66.

——, 1954b: Die Abhängigkeit der charakteristichen Grö Ben einer thermisch bedingten Zirkulation von den die näheren Umstände beschreibenden Parametorn im falle gewisser quasistationärer Zirkulationen. *Z. Meteor.*, **8**, 289–303.

——, 1955: Über thermisch bedingte Zirkulationen mit jährlicher periode (Beiträge Zum Monsunproblem I.) *Z. Meteor.*, **9**, 326–345.

Brown, J. A., 1964: Diagnostic study of tropospheric diabatic heating and the generation of A.P.E. *Tellus*, **16**, 371–388.

Brunt, D., 1941: *Physical and Dynamical Meteorology*. New York, Cambridge University Press, 428 pp. (see pp. 252–257).

Charney, J. G., and A. Eliassen, 1949: A numerical method for predicting the perturbation of the middle latitude westerlies. *Tellus*, **1**, 38–54.

Coulson, C. A., 1931: Geostrophic winds. *Quart. J. Roy. Meteor. Soc.*, **57**, 161–162.

Delsol, F., K. Miyakoda, and R. H. Clarke, 1971: Parameterised processes in the surface boundary layer of an atmospheric circulation model. *Quart. J. Roy. Meteor. Soc.*, **97**, 181–209.

Derome, J., and Wiin-Nielson, A., 1971: Response of a middle-latitude model atmosphere to forcing by topography and stationary heat sources. *Mon. Wea. Rev.*, **99**, 564–576.

Dickinson, R. E., 1971: Analytic model for zonal winds in the tropics. *Mon. Wea. Rev.*, **99**, 511–523.

Döös, B. R., 1961: The scale of non-adiabatic heating as a factor in cyclogenesis. *J. Meteor.*, **18**, 1–8.

——, 1962: Influence of exchange of sensible heat with the earth's surface on the planetary flow. *Tellus*, **14**, 133–147.

Everson, P. J., and D. R. Davies, 1972: Ekman boundary layer interaction in a numerical model of general circulation. *Quart. J. Roy. Meteor. Soc.*, **98**, 412–419.

Fisher, P. W. A., and Wiin-Nielson, 1971: On baroclinic instability of ultralong waves. *Tellus*, **23**, 269–283.

Godbole, R. V., 1973: Numerical simulation of Indian summer monsoon. *Ind. J. Meteor & Geophys.*, **24**, 1–14.

Haltiner, G. J., and F. L. Martin, 1957: *Dynamical and Physical Meteorology*. New York, McGraw-Hill Book Co., 470 pp. (see p. 242).

Jeffreys, H., 1926: On the dynamics of geostrophic winds. *Quart. J. Roy. Meteor. Soc.*, **52**, 85–104.

Kuo, H. L., 1956: Forced and free axially symmetric convection produced by differential heating in a rotating fluid. *J. Meteor.*, **13**, 521–527.

Leith Holloway, J., and S. Manabe, 1971: Simulation of climate by a global general circulation model: I. Hydrologic cycle and heat balance. *Mon. Wea. Rev.*, **99**, 335–370.

Lorenz, E. N., 1960: Energy and numerical weather prediction. *Tellus*, **12**, 364–373.

Manabe, S., and J. Smagorinsky, 1967: Simulated climatology of a general circulation model with a hydrologic cycle II: Analysis of the tropical atmosphere. *Mon. Wea. Rev.*, **95**, 155–169.

——, ——, and R. F. Strickler, 1965: Simulated climatology of a general circulation model with a hydrologic cycle. *Mon. Wea. Rev.*, **93**, 769–798.

——, ——, J. Leith Holloway, Jr., and H. M. Stone, 1970: Simulated climatology of a general circulation model with a hydrologic cycle III. Effects of increased horizontal computational resolution. *Mon. Wea. Rev.*, **98**, 175–213.

Mintz, Y., and A. Arakawa, 1965: Very long-term global integration of the primitive equations of atmospheric motion. Geneva, *WMO Tech. Note* No. 66, 141–167.

Murakami, T., 1957a: Seasonal variation of mean vertical velocity and atmospheric heat sources over Far East from spring to summer. *Papers Meteor. Geophys., Japan*, **7**, 358–376.

——, 1957b: Mean vertical velocity and heat supply during rainy season near Japan. *Papers Meteor. Geophys., Japan*, **8**, 109–132.

——, 1967: Vertical transfer of energy due to stationary disturbances induced by topography and diabatic heat sources and sinks. *J. Meteor. Soc. Japan*, Ser. 2, **45**, 205–230.

——, 1972: Equatorial tropospheric waves induced by diabatic heating. *J. Atmos. Sci.*, **29**, 827–836.

Pasquill, F., 1962: *Atmospheric Diffusion*. London, D. van Nostrand Co. Ltd., 297 pp.

Phillips, N. A., 1956: General circulation of atmosphere, A numerical experiment. *Quart. J. Roy. Meteor. Soc.*, **82**, 123–164

Pisharoty, P. R., and G. C. Asnani, 1958: Dynamical theories of the monsoon—a survey. *Proceedings of Symposium on Monsoons of the World*, New Delhi, 129–134.

Ramage, C. S., 1971: *Monsoon Meteorology*. International Geophysics Series Vol. 15, New York, Academic Press, 296 pp.

Reed, R. J., and E. E. Recker, 1971: Structure and properties of of synoptic-scale wave disturbances in equatorial W. Pacific. *J. Atmos. Sci.*, **28**, 1117–1133.

Rossby, C. G., and R. B. Montgomery, 1935: The layer of frictional influence in wind and ocean currents. *Pap. Phys. Oceanog., Meteor.*, M.I.T. and Woods Hole Oceanographic Institution, **3**, No. 3.

Saltzman, B., 1965: Theory of the winter-average perturbations in the troposphere and stratosphere. *Mon. Wea. Rev.*, **93**, 195–211.

Sankar Rao, M., and B. Saltzman, 1969: Steady state theory of global monsoons. *Tellus*, **21**, 308–330.

Smagorinsky, J., 1953: The dynamical influence of large-scale heat sources and sinks on the quasistationary mean motions of the atmosphere. *Quart. J. Roy. Meteor. Soc.*, **79**, 342–366.

——, 1963: General circulation experiments with the primitive equations: I. The basic experiment. *Mon. Wea. Rev.*, **91**, 99–164.

Webster, P. J., 1972: Response of the tropical atmosphere to local steady forcing. *Mon. Wea. Rev.*, **100**, 518–541.